JOURNAL OF MATERIALS SCIENCE 39 (2004) 4157–4170

Elastic and elastoplastic response of thin copper foil

H. D. MERCHANT
Gould Electronics Inc., Eastlake, OH 44095, USA

G. KHATIBI, B. WEISS*
Inst. of Materialphysics, University of Vienna, Vienna, Austria
E-mail: weissb@ap.univie.ac.at

The tensile elastic, elastoplastic and low strain plastic parameters of the 12–35 μm thick rolled (*R*) and electrodeposited (ED) copper foils have been characterized between 296 and 573 K and after an anneal exposure at up to 1173 K. At 296 K, all parameters are inversely proportional to grain size but the thermal effects dominate at the higher temperatures. For the *R* foils, the temperature coefficient of elastic modulus (*E*) is more or less identical to that for the bulk copper. For the ED foils, the coefficient increases with decreasing grain size; this effect is presumably related to the characteristic point defect structure generated during deposition. A significant grain growth ensues upon annealing but the post-anneal grain size has little effect on *E*; for the *R* foil, however, *E* decreases sharply with the anneal induced emergence of new crystallogrpahic textures with orientations near ⟨100⟩ . The tangent modulus (E_t) in the elastoplastic regime decreases with strain and with temperature, a very large drop in E_t with anneal temperature suggests that both the diminution of dislocation activity and the texture modification are the contributory factors. It is argued that the strain hardening parameter (*n*) in the elastoplastic regime, and the strain rate hardening parameter (*m*) and the flow stress in the low strain plastic regime influence the handling damage to the thin foil.

1. Introduction

The elastic response of thin film or foil has been investigated by a variety of techniques: X-ray diffraction [1–3], bending [4, 5] (cantilever beam [6], bi-axial [7], three-point [8]), indentation [9] (nano- [10], spherical tipped [11]), bulging [12, 13] sonics [14], elastic waves [15], surface acoustics [16–18], vibrating reed [19, 20], dynamic mechanical analyzer (DMA) [21] and tensile loading [1, 22–25]. The most characterizations, however, have been at room temperature. The tensile technique, in particular, is amenable to tests at higher temperatures [23–25]; furthermore, it permits specific examination of the elastoplastic (between proportional limit and plastic yielding) and the low strain post-yield responses.

The freestanding copper foil has been investigated in tensile mode to a limited extent [1, 22, 23, 25]. The reported room temperature modulus values are often lower than those for the bulk copper [26]. The grain size, the nature of grain boundaries, especially for the vapor or electrodeposited foil, and the incidence of micropores and microcracks are prone to affect the modulus [15, 27]. The crystallographic texture, likewise, can have a significant effect since the modulus of copper is direction specific [28, 29]. For example, the modulus in the ⟨111⟩ direction is 2.9 times greater than that in the ⟨100⟩ direction. The grain orientation as well as the grain shape, in the as fabricated and annealed conditions, can influence the elastic modulus [30].

The conventional tensile testing of copper foil utilizes the crosshead movement monitor to ascertain strain. However, this procedure overestimates strain in the elastic regime, with a slight bending of the stress-strain (σ-ε) curve; the net result is (i) a low apparent elastic modulus (*E*), (ii) a gradual elastic to plastic yield transition and (iii) a somewhat imprecise definition of yield level (σ_y, ε_y). The *E* and σ_y values for cold rolled 6 mm copper plate between 296 and 723 K, using contact extensometer, have been determined by Munse and Weil [26]. Employing a non-contact optical strain tracking system, essential for the fragile foil sample, Fox [23] has obtained credible modulus resutls for the 75–145 μm thick electrodeposited (ED) copper (Cu) foil between 296 and 448 K. Similar results for the 30.5 μm ED Cu foil have been obtained by Fu and Ume [25] but with a more pronounced test temperature effect on *E*. A more accurate tensile characterization of E, σ_y and σ-ε curve in the elastoplastic region, however, requires a loading/unloading technique described elsewhere [31] (see Fig. 1).

*Author to whom all correspondence should be addressed.

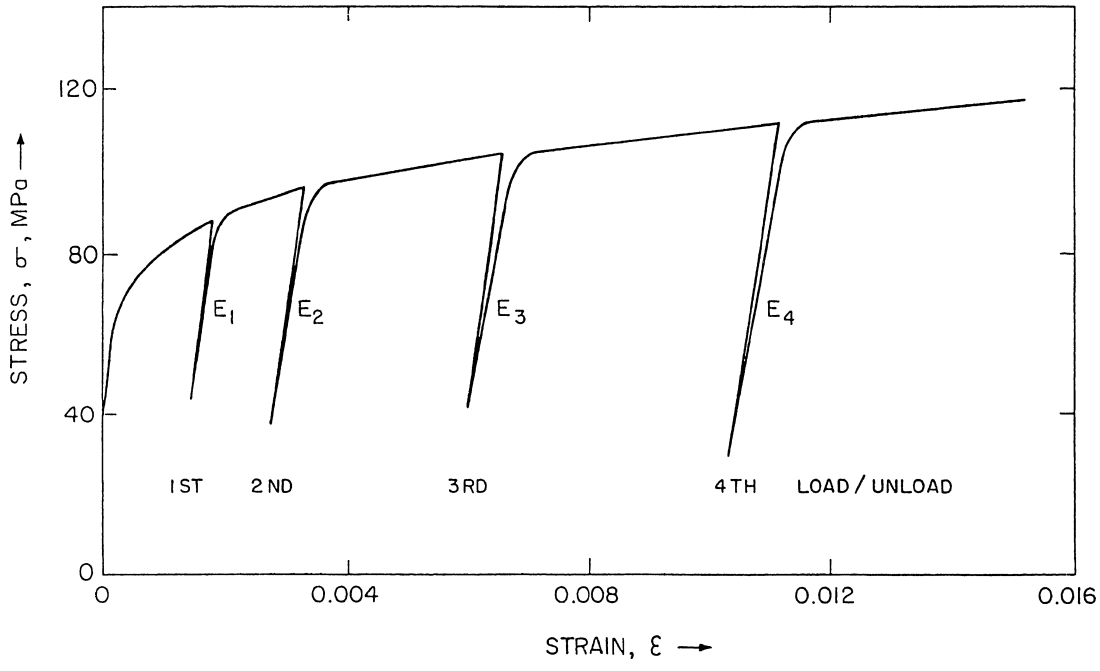

Figure 1 Loading/Unloading procedure for elastic modulus determination.

The primary application for the thin freestanding electrodeposited and rolled copper foils is in the electronic packaging field. Rather than examining the laboratory prepared foil samples, the commercially processed foils, designated by specific grades, are investigated in this paper. They represent a range of grain structures, crystallographic textures and thermal stabilities (of structure and texture), and should help relate the elastic and elastoplastic parameters to the microstructure. During service at and above room temperature, the thin foil is prone to a variety of failure modes: buckle, dent, wrinkle, warp or curl (during lamination to polymeric substrate) [32]. One of the aims of this study is to determine the mechanical parameters which govern these failure modes [32].

2. Materials

Four grades (AM, low profile GR3, high profile GR3 and DF) of electrodeposited (ED) and three grades (TPC, Ag-TPC and OFC) of rolled (R) 12–35 μm thick freestanding copper foils in the as-fabricated and annealed (to 1173 K, in argon) states are characterized. The average mid-thickness planar grain size, determined by the transmission electron microscopy (TEM), prior to and following a 200–300s thermal exposure to 573 K, for each foil grade is shown in Table I. Furthermore, the characteristic planar grain coarsening curves, following a 1800s thermal exposure are presented in Fig. 2 for the 18 μm DF, TPC and OFC grade foils. Here the planar grain size is determined by the scanning electron (SEM) and optical microscopy techniques. Typical grain structures of the ED and *R* foils before and after anneal exposure are illustrated in Fig. 3.

For the ED foils, thermal anneal (loss of hardness, reduction in dislocation density) is accompanied by a continuous *in-situ* grain growth [33]; for the *R* foils, rapid anneal softening at about 423 K occurs in concert with discontinuous recrystallization, whereby the new grains form at the expense of the old [34]. For the ED foils, the grain structure is generally equiaxed; except for the high profile GR3 foil where some *z* (thickness)—direction grain extension is observed. For the *R* foils, the grains are flattened during rolling; in the post-anneal state, the new equiaxed grains are formed. The grain

TABLE I Average grain size of copper foil (μm)

Commercial foil		Thickness (μm) →	12				18				35			
Type*	Grade	Temp.** (K)	296	373	473	573	296	373	473	573	296	373	473	573
ED	AM		–	–	–	–	–	–	–	–	0.4	0.4	0.5	2.0
ED	Lo Profile GR3		–	–	–	–	–	–	–	–	0.5	0.5	0.8	1.5
ED	Hi Profile GR3		–	–	–	–	–	–	–	–	2.0	2.0	3.0	3.5
ED	DF		0.3	0.4	1.8	2.5	0.4	0.6	1.0	1.2	0.7	0.8	1.2	1.5
R	TPC		2.5	3.0	6	8	3.5	4.0	6	8	4.5	4.5	6	8
R	OFC		–	–	–	–	2.5	3.0	6	8	–	–	–	–

*ED = electrodeposited mid-thickness planar grain size; *R* = rolled, planar rolling direction grain size.
**200–300 s thermal exposure.

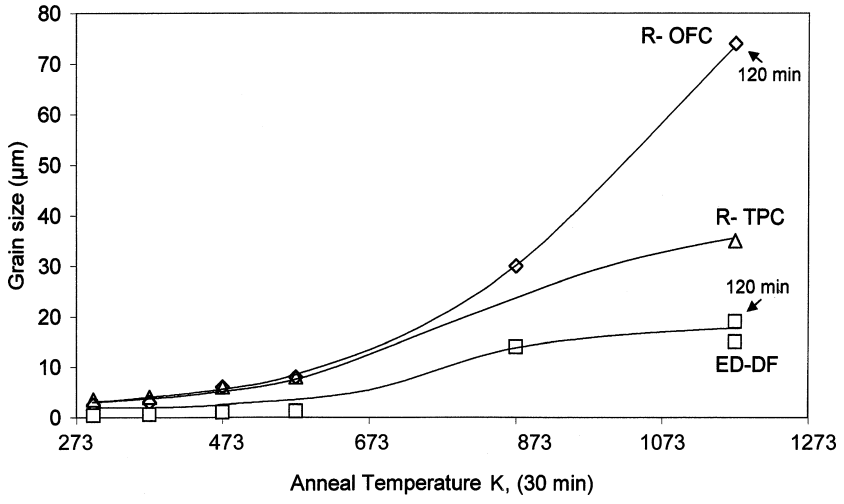

Figure 2 Anneal induced grain coarsening for 18 μm DF, TPC and OFC foils.

structure and the average grain size for the Ag-TPC and OFC foils are virtually identical.

Several additional aspects of the grain structure of thin copper foil should be emphasized. For the ED foil, the "pseudo" grain boundaries in the as-deposited state are poorly and unevenly delineated. This aspect of grain boundaries becomes particularly acute in the cross-section view where the grain structure is complex and difficult to decipher. Upon annealing, the grain boundary delineation improves remarkably. However, when the grain size becomes comparable with the foil thickness, following the anneal induced grain growth, the boundaries interact with the free foil surfaces and a "bamboo" grain structure ensues. For the *R* foil, the "pancake" character of the grains is retained after recrystallization and the planar grain growth occurs more or less unimpeded by the foil surfaces. A bamboo grain structure after grain growth is less prone to develop. Further details of the grain structure for the ED and *R* foils are discussed in a companion paper [35].

Among the ED foils, the AM foil displays a totally random grain orientation; the high profile GR3 is characterized by a strong ⟨220⟩ fiber texture, with over 90% of the grains oriented along the fiber axis [36]. The low profile GR3 and DF foils show a weak ⟨220⟩ texture, the random grain fraction is in excess of 80%. For all ED foils, the textures are stable to 1173 K; the anneal induced grain growth leaves the original as-deposited textures unaltered. The *R* foils show strong deformation textures which upon annealing transform to the recrystallization textures, as illustrated in Table II for the 18 μm foils. The texture transformation, however, does not coincide with the recrystallization process; for the TPC foil, the textures are stable to about 873 K, 1800s thermal exposure, whereas for the Ag-TPC and OFC foils, the texture transformation occurs closer to the recrystallization temperature. Further details of the crystallographic texture for the ED and *R* foils are discussed in the companion paper [35].

3. Experimental: Tensile tests

Mechanical properties of the foil specimens of 60 mm length were determined employing a microtensile testing apparatus (Messphysik, Austria). The apparatus is equipped with a non-contacting optical laser speckle correlation system for strain measurements [37], and the force is measured with a 100 N capacity (type TCA) load cell calibrated with standard weights. The foils were glued into specially designed grips using a jig to prevent deformation of the foils during handling. The specimens were aligned using an x-y stage with visual control on the monitor. A small initial load was applied to straighten the foil specimens. The entire testing device was mounted on an optical table to minimize the influence of detrimental vibrations. During

TABLE II Volume fractions of ideal texture components for 18 μm *R* foils

Sample	Anneal	(i) Brass	(ii) S	(iii) Cu	(iv) Cube	(v) *r*-Cube	(vi) Goss	% (i + ii + iii) (i + ⋯ + vi)	% (iv + v + vi) (i + ⋯ + vi)	(vii) Random
TPC	–	14.6	26.4	11.8	5.5	0.5	3.4	84.9	15.1	37.8
Ag-TPC	–	23.8	28.2	8.0	2.6	0.2	2.2	92.3	7.7	35.0
OFC	–	28.1	26.2	7.4	2.0	0.7	1.6	93.5	6.5	34.1
TPC	453 K, 30 min	5.0	15.2	4.9	10.4	2.1	2.6	62.4	37.6	59.9
Ag-TPC	”	2.9	12.8	2.4	17.9	2.0	2.9	44.3	55.7	59.1
OFC	”	3.0	10.2	3.2	16.7	1.4	3.2	43.5	56.5	62.2
TPC	1173 K, 30 min	5.4	8.5	1.5	12.8	0.8	2.6	48.7	51.3	68.5
OFC	”	4.2	11.6	2.0	16.9	1.7	3.4	44.7	55.3	60.2

Brass: {110} ⟨112⟩; S: {132} ⟨643⟩; Cu: {123} ⟨111⟩; Cube: {100} ⟨001⟩; *r*-Cube: {100} ⟨011⟩; Goss: {110} ⟨001⟩.

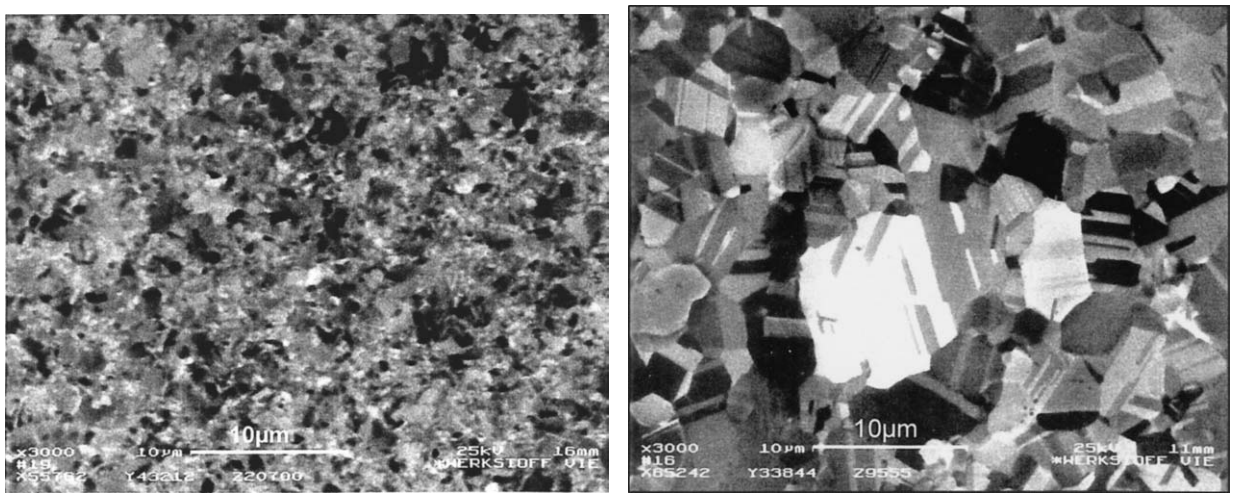

(a) (b)

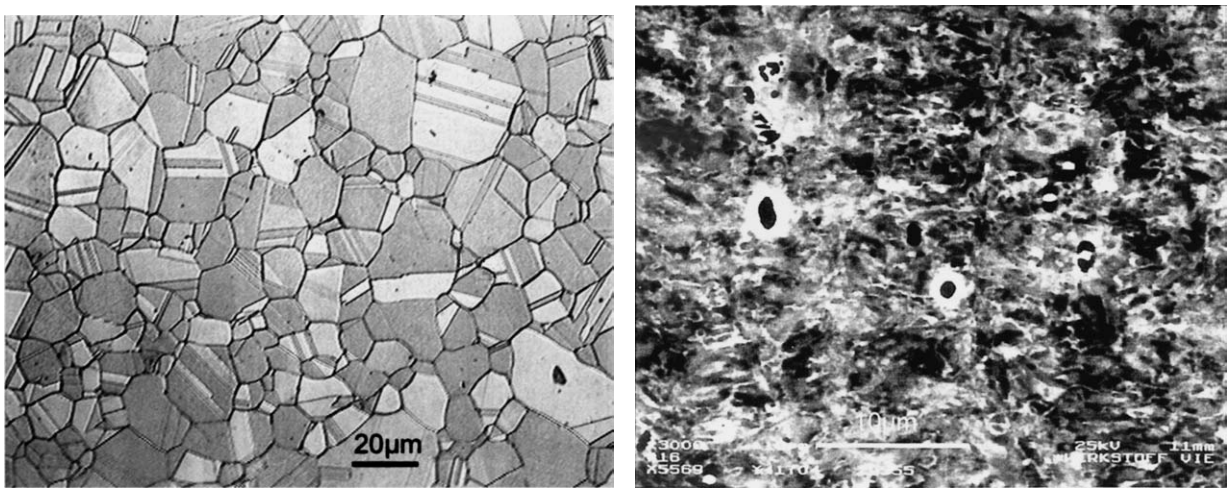

(c) (d)

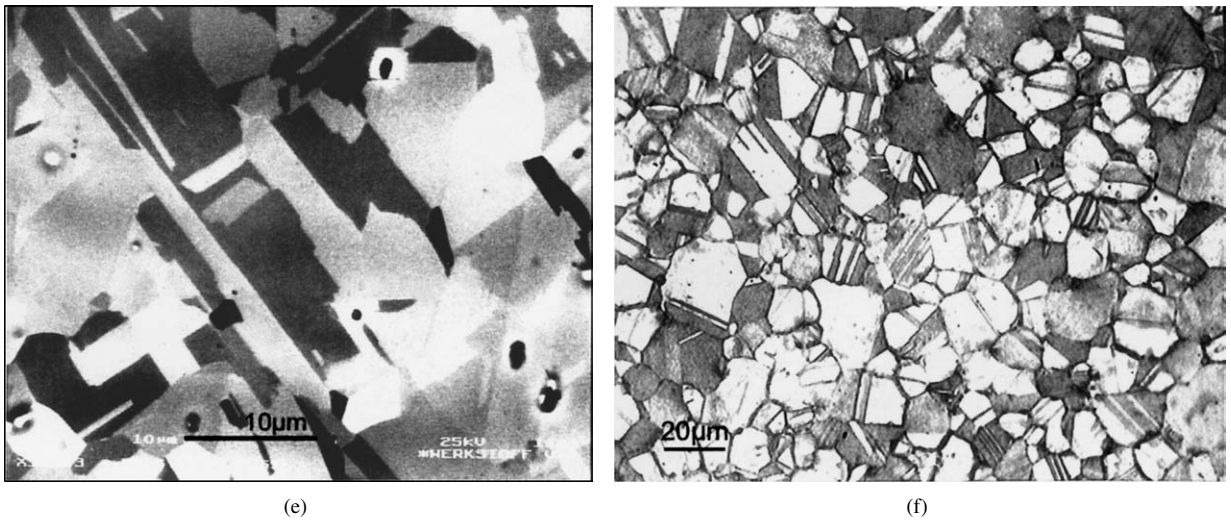

(e) (f)

Figure 3 Typical planar grain structures prior to and following anneal exposure for 18 μm ED and *R* foils. ED: (a) as received; (b) 573 K/30 min; (c) 1173 K/120 min *R*(TPC): (d) as received; (e) 573 K/30 min; and (f) 1173 K 120 min.

a displacement controlled tensile test at 10^{-4}/s strain rate, the sample is illuminated by two collimated laser beams of 15 mw power and the laser speckle patterns are formed on the specimen surface.

A schematic of the optical arrangement, consisting of the illuminating system and two displacement recording systems, is presented in Fig. 4. The displacement recording is performed by two lenses (separated by a base length of 40 mm) with a selectable focal length and standard charge coupling devices (CCD cameras) feeding the signals of the images into a personal computer based frame grabber, where the signal processing occurs. The strain values are obtained on-line from the cross-correlation function between sequential images.

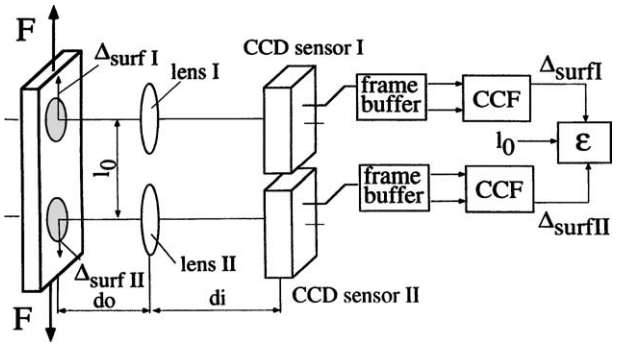

Figure 4 Set-up for the laser speckle extensometer (schematic).

Further details of the laser extensometer are described in Ref. [37]. The resolution of the system for the selected sample gauge length of 40 mm is $5 \cdot 10^{-5}$ for the strain and 0.01 MPa for the stress.

The elastic and elastoplastic parameters were determined at test temperatures up to 573 K. In order to hold the test temperature at a constant level, a regulated stream of heated air was blown around the samples; holding the maximum temperature error within ±5°C. The parameters were (i) elastic modulus E, (ii) strain hardening parameter n ($\sigma \sim \varepsilon^n$), obtained by regression analysis between a range of strains, (iii) tangent modulus E_t, slope $d\sigma/d\varepsilon$ of σ-ε curve in the elastoplastic region and (iv) yield stress σ_y (stress at 0.2% cut-off strain). Several loading/unloading stages, illustrated in Fig. 1, produce a number of E readings, within 5% scatter, which are averaged to develop a data point. The n and E_t values are for ε between 0.05 and 0.2%; E_t and σ_y are averages of several readings within 2% scatter.

Using a conventional tensile tester described before [33, 38] and monitoring the tester crosshead movement, n was determined at 10^{-5}/s strain rate between 0.1 and 1% offset strain. The strain rate hardening parameter m ($\sigma \sim \dot{\varepsilon}^m$) at a given strain, determined between the 0.2% (yield point) and 0.55% offset strain, was characterized by an abrupt change in strain rate [39] from 10^{-5} to 10^{-4} s^{-1}. Here m [=log (σ_2/σ_1)/log $(\dot{\varepsilon}_2/\dot{\varepsilon}_1)$] at a specific strain is calculated by using the extrapolation procedure, to obtain optimum m, discussed in Ref. [39].

4. Results

4.1. Elastic modulus (E)

Fig. 5 shows the effect of test temperature on E for the 35 μm ED and R foils. The indicated grain sizes are the initial pre-test values; during thermal equilibration at the test temperature and during load cycling, considerable grain coarsening ensues as shown in Table I and Fig. 2. The fine grain size ED foils (AM and low profile GR3) have relatively large E at 296 K but also a large loss of E with test temperature; at 573 K, the cumulative loss of E is about 65%, a three to five fold grain growth is in part responsible for the loss. By comparison, the (R) TPC foil with an initially coarse grain structure shows a relatively small drop in E to 473 K, followed by a rapid drop in the 473–573 K range. Note that at 573 K the smallest (initial) grain size foils have the lowest E.

For the 12–35 μm (ED) DF, (R) TPC and (R) OFC foils, Fig. 6 shows the effect of up to 1173 K, 1800s anneal on E tested at 296, 373 and 473 K. A small increase in E with decreasing foil thickness is observed. For the DF foil, the thermal exposure causes little change in E with (anneal) temperature, in spite of the fact that an intense grain growth occurs above about 673 K [35]. For the R foil, a sharp drop in E at 296 and 373 K test temperatures is observed. For the OFC foil, the drop occurs in the 423–473 K interval that is somewhat above the 403–423 K thermal softening (decrease in dislocation density) range. For the TPC foil, the drop occurs around 873 K but is smaller (than for the OFC foil). The

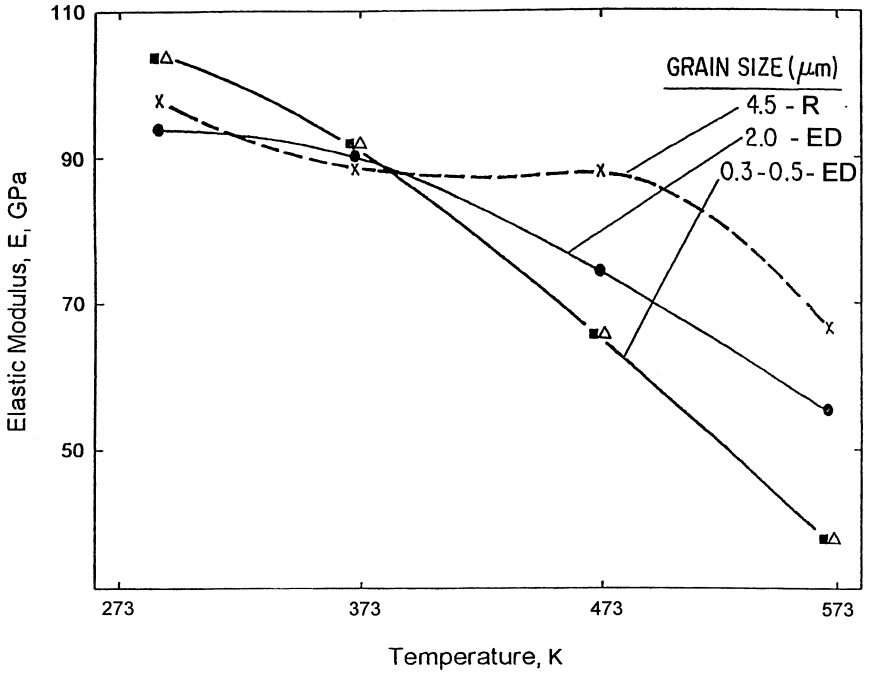

Figure 5 Effect of test temperature on elastic modulus for 35 μm copper foils.

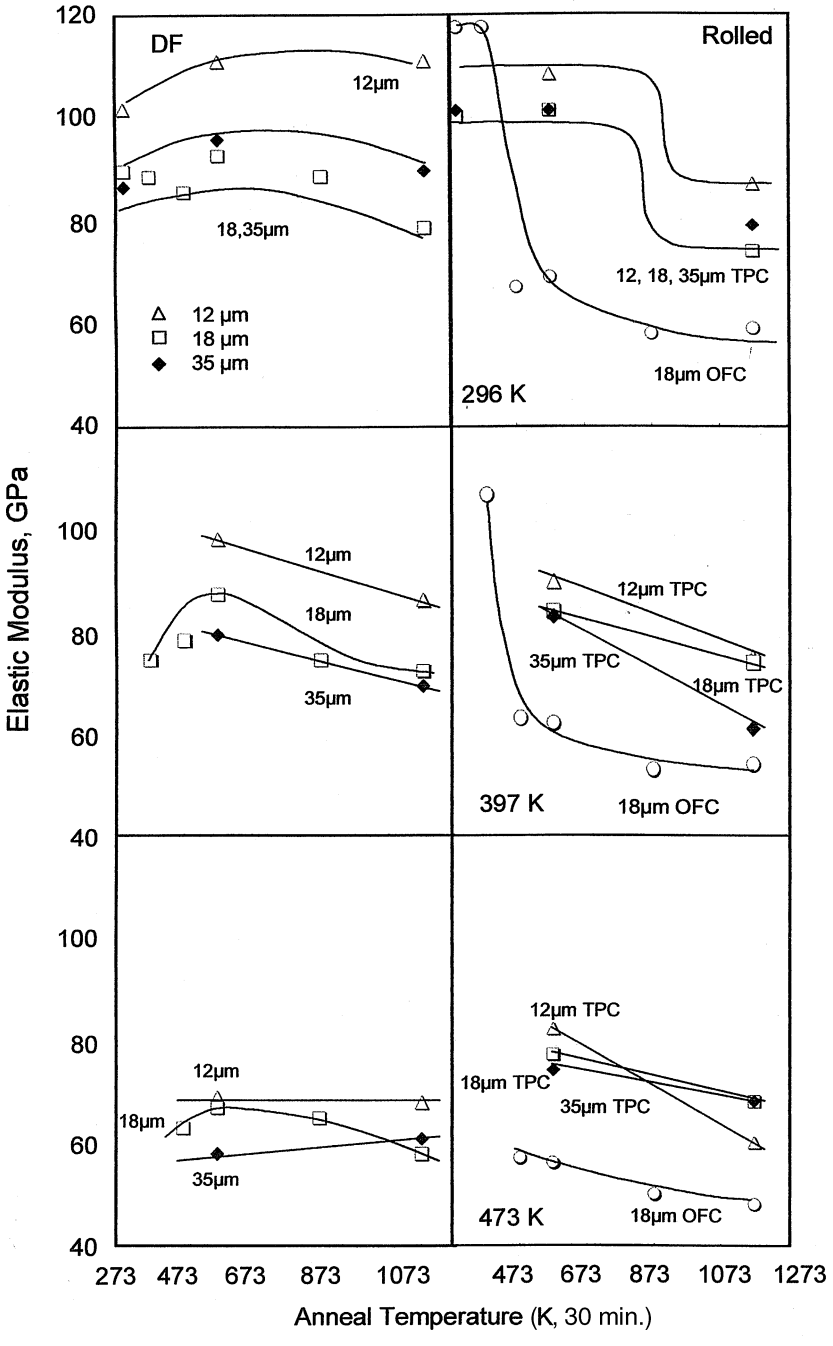

Figure 6 Effect of 1800s anneal on elastic modulus for 12–35 μm DF and *R* Foils tested at (a) 296 K, (b) 373 K and (c) 473 K.

effect of test temperature for the TPC foil is similar to the results reported in Fig. 5. These significant reductions in E are apparently related to the generation of anneal induced textures near the ⟨100⟩ orientation (see Table II).

4.2. Elastoplastic: Strain hardening parameter (n)

The effect of test temperature on n in the 0.05–0.20% offset strain range for the 35 μm ED and R foils is shown in Fig. 7. The ED foils have much higher n (than the R (TPC) foil); however, the n decreases with temperature and at 573 K for all foils it approaches about 0.1 level. The finer grain size foil has a higher n but the effect of grain size on n decreases with increasing test temperature. The effect of annealing on n for the 18 μm (ED) DF and (R) OFC foils is shown in Fig. 8. The n decreases with the anneal temperature; the DF foil has a higher n (than for the OFC foil), especially up to about 573 K (anneal) temperature. For all foils after 1173 K anneal, a coarse grain structure (grain size comparable to the foil thickness) is formed [35] and the n approaches about 0.1 level.

4.3. Elastoplastic: Tangent modulus (E_t)

The effect of strain on E_t is presented in Figs 9 and 10 for the 296/373 K and 473/573 K test temperatures respectively. As the strain approaches the yield point (0.2% offset), the E_t, as expected, decreases gradually. The grain size has an inverse effect on E_t but with increasing test temperature the thermal contribution to E_t dominates the grain size effect. At 573 K, the E_t tends

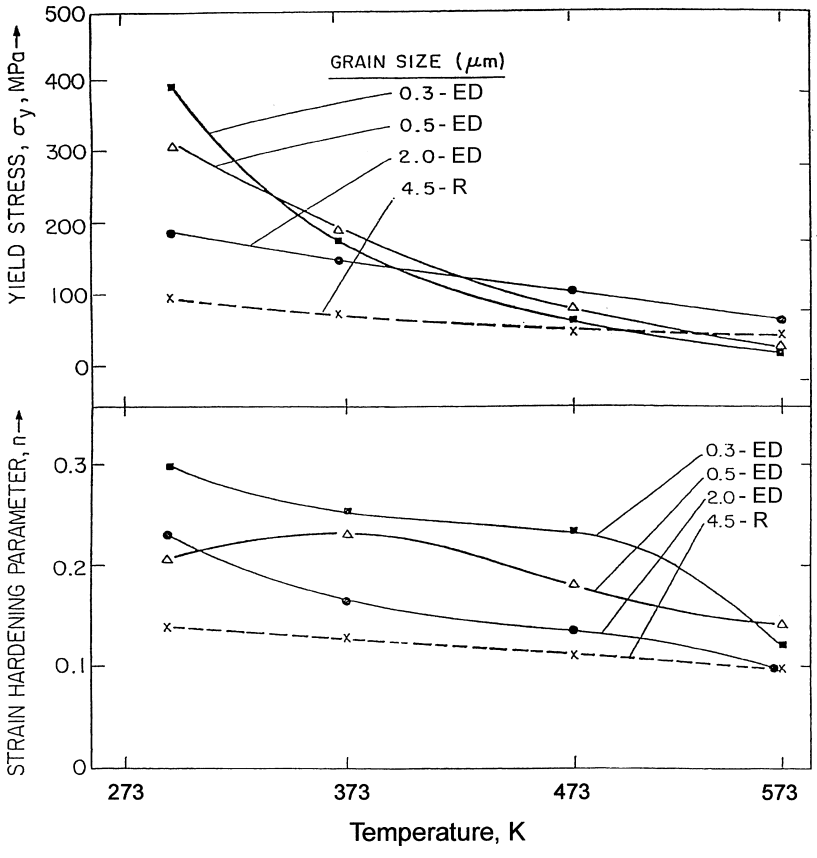

Figure 7 Effect of test temperature on (a) yield stress, (b) strain hardening parameter for 35 μm copper foils.

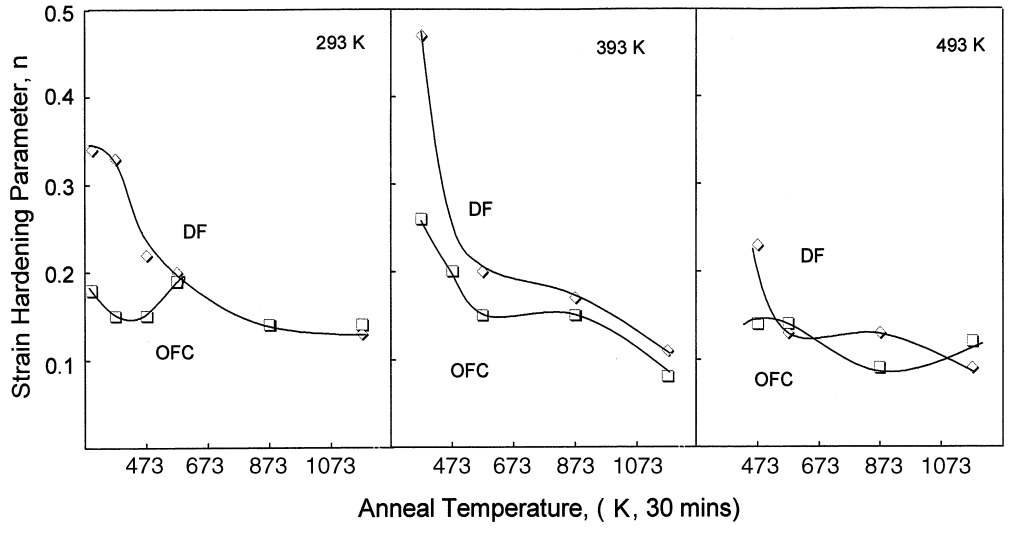

Figure 8 Effect of 1800s anneal on strain hardening parameter for 18 μm DF and OFC foils.

to a very low 2–5 GPa value, indicating a flattening of the elastoplastic σ-ε curve with increasing temperature. E_t is much smaller than E; at 473 K, E_t is about 1% of the E value.

Fig. 11 shows the effect of annealing on E and E_t, for the 18 μm ED (DF) and (R) OFC foils tested at 296 and 473 K. For the OFC foil and 296 K test, an anneal around 473 K results in a large E_t drop (but a relatively small loss of E); it is presumably related to the texture transformation (to near ⟨100⟩ orientations) and to the recrystallization (reduction in dislocation density). For the DF foil, the anneal effect is gradual over the whole (anneal) temperature range; since no texture change occurs with temperature, the diminution of E_t is apparently related to the sluggish anneal (reduction in dislocation density, grain coarsening) effect.

4.4. Yield stress (σ_y)

The effect of test temperature on yield stress for the 35 μm ED and R foils is shown in Fig. 7. The grain size effect on σ_y is evident at 296 K; however, σ_y decreases with temperature and this effect is greatest for the smallest (initial) grain size foil. At 573 K, the σ_y approaches 40–90 MPa range. For the 18 μm (ED) DF

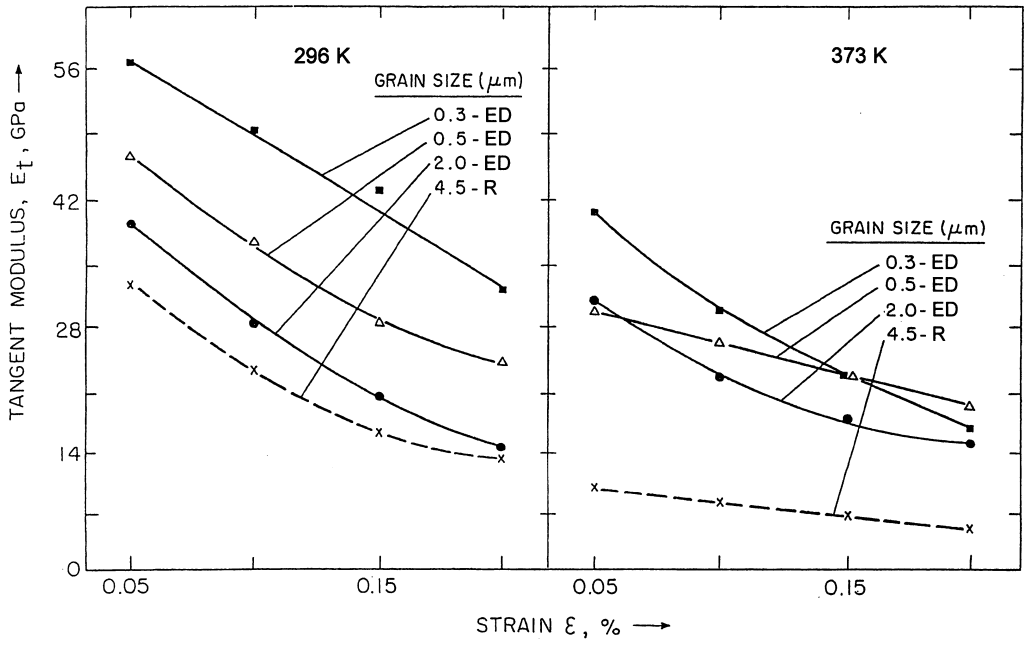

Figure 9 Effect of strain in elasto-plastic region on tangent modulus for 35 μm copper foils tested at 296 K and 373 K.

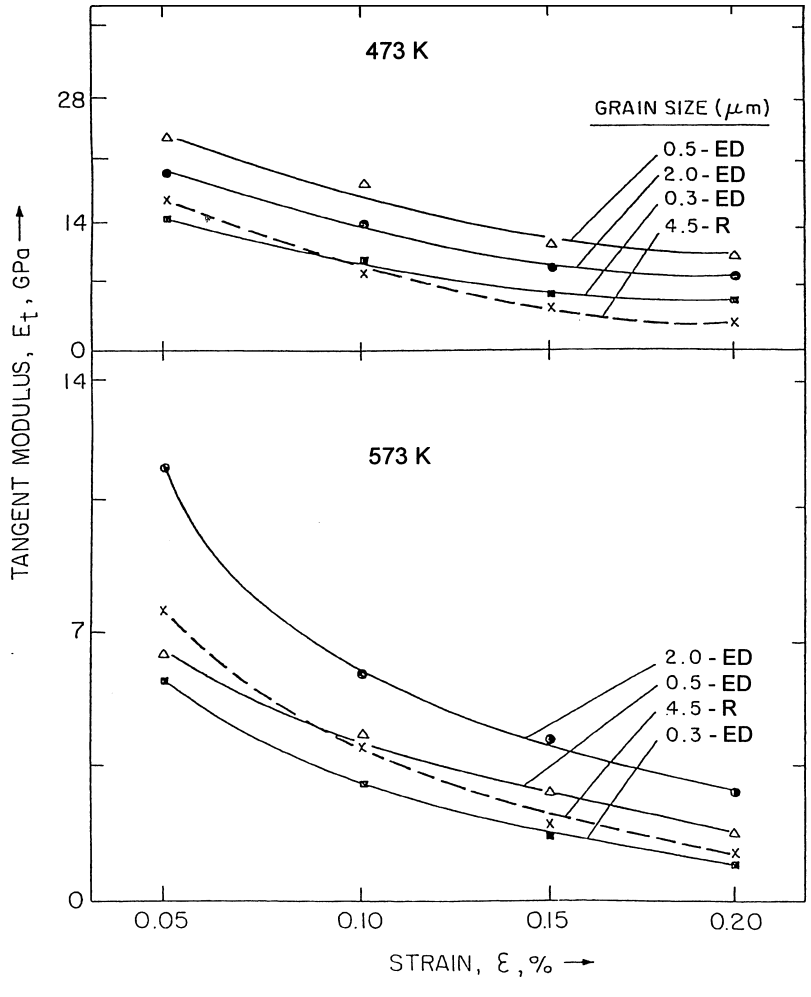

Figure 10 Effect of strain in elasto-plastic region on tangent modulus for 35 μm copper foils tested at 473 K and 573 K.

and *R* (OFC) foils, the effect of annealing for the 296, 373 and 473 K tests is presented in Fig. 12. For the OFC foil, the precipitous drop in σ_y (recrystallization reaction) is followed by a flattening of the anneal curve. A more gradual softening for the DF foil corresponds to its characteristic *in situ* grain growth with increasing anneal temperature [33]. After 1173 K anneal, σ_y for both foil types approaches a very low 20–30 MPa level which corresponds to grain size between 20–60 μm (Fig. 2).

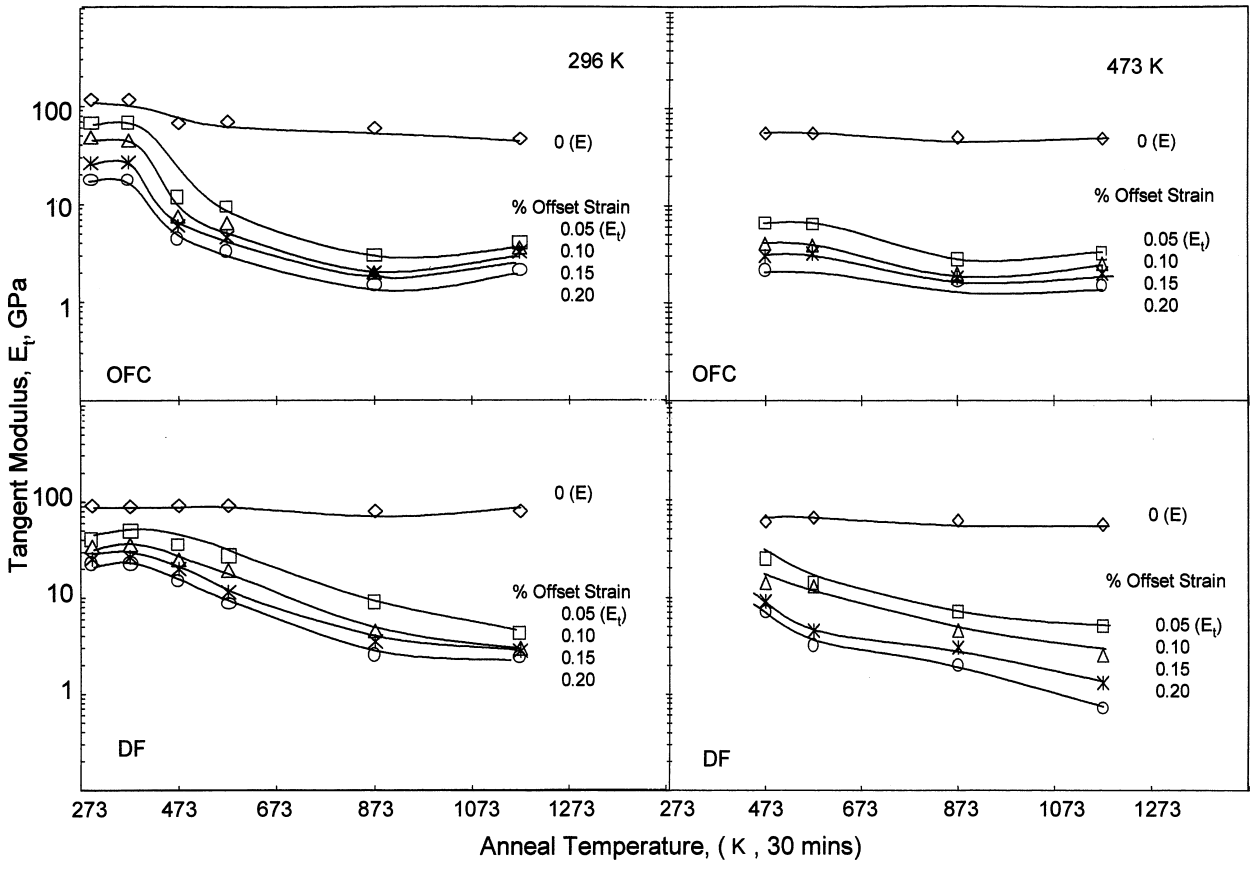

Figure 11 Effect of 1800s anneal on tangent modulus for 18 μm OFC and DF foils tested at (a) 296 K and (b) 473 K.

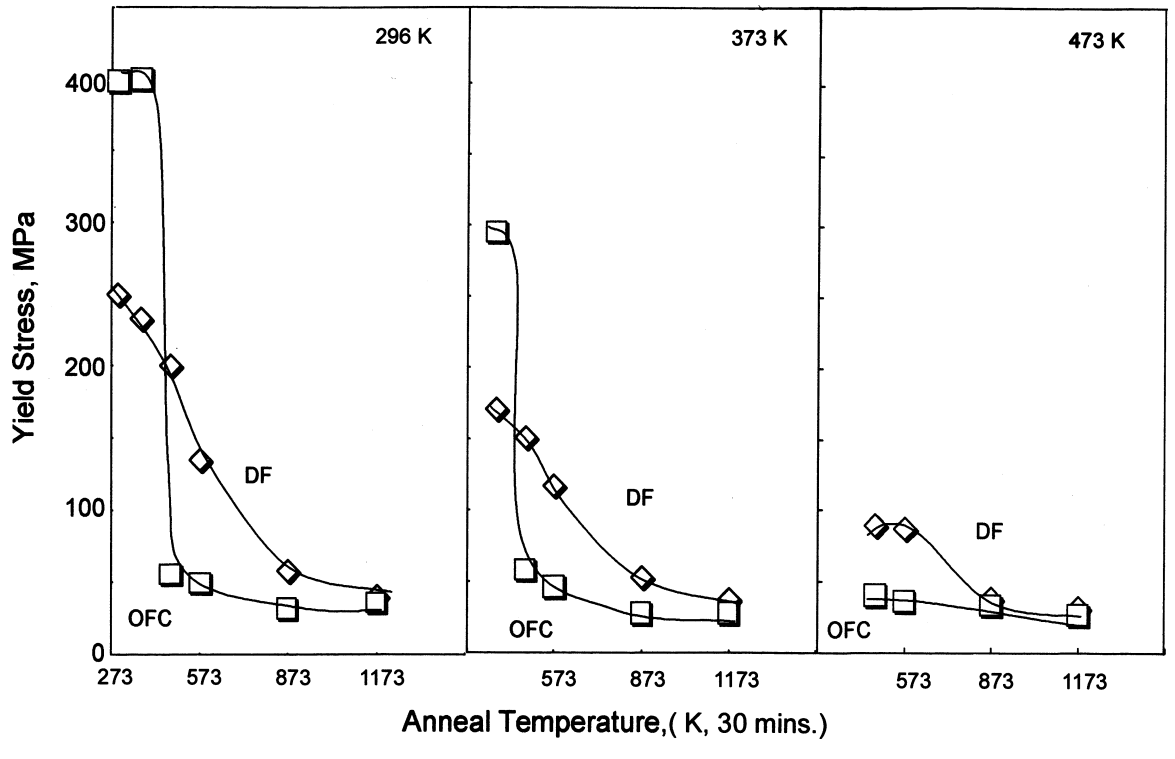

Figure 12 Effect of 1800s anneal on yield stress for 18 μm OFC and DF foils tested at (a) 296 K, (b) 373 K and (c) 473 K.

4.5. Low strain regime

Four 35 μm high profile (ED) GR 3 foils, each processed somewhat differently but with roughly similar grain structure and crystallographic texture, are characterized for strain hardening and strain rate hardening in the 413–453 K test temperature range. Fig. 13 shows the 453 K σ-ε (logarithmic) plots between 0.1 and 1% offset strain; the slope of each plot, or of a segment of the plot, defines n. The two high flow stress foils have a relatively low elastoplastic n (0.19–0.20); the

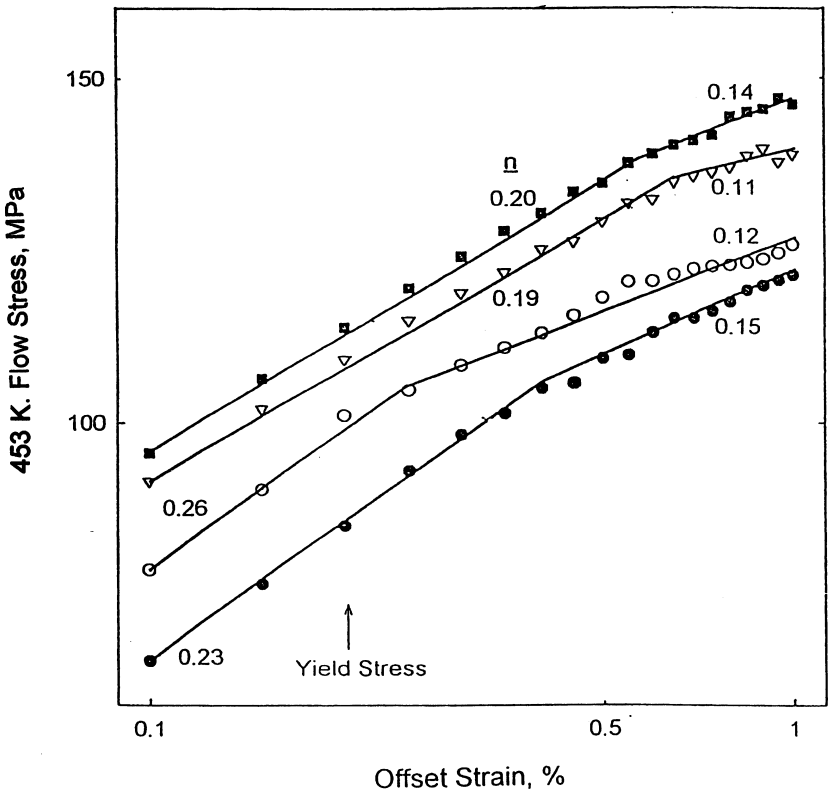

Figure 13 Effect of offset strain on flow stress for 35 μm copper foils tested at 453 K.

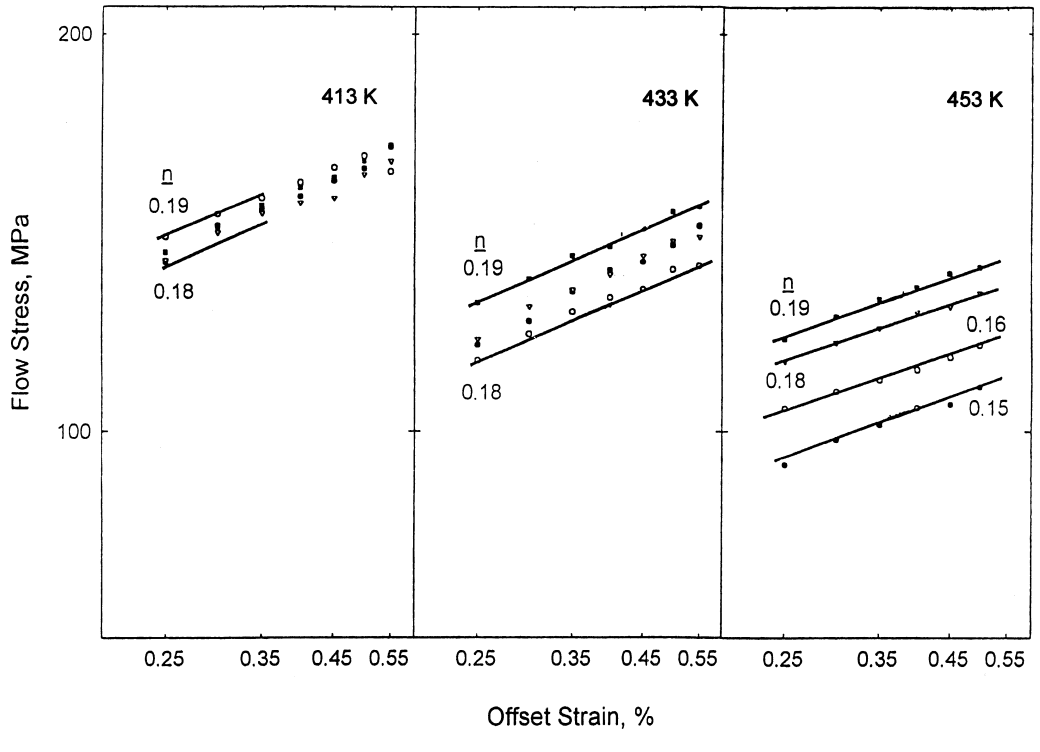

Figure 14 Effect of plastic offset strain on flow stress for 35 μm copper foils tested at (a) 413 K, (b) 433 K and (c) 453 K.

two low flow stress foils have a relatively low "low strain" plastic n (0.12–0.15). Fig. 14 shows the σ-ε (logarithmic) plots in the 0.25–0.55% offset plastic strain regime tested at 413, 433 and 453 K. Only at 453 K, the foils can be distinguished as the low and high flow stress types, the former displaying a somewhat higher n (0.18–0.19 versus 0.15–0.16).

Fig. 15 shows the strain rate hardening parameter m, determined by the strain rate change method [39], as a function of plastic offset strain for the two (high and low flow stress) foil types tested at 413, 433 and 453 K. The uncommonly high m is perhaps due to the very low strain levels and the fine grain structure of the foils. The m decreases with strain and with test temperature, reaching a more conventional value of 0.05 for the lower

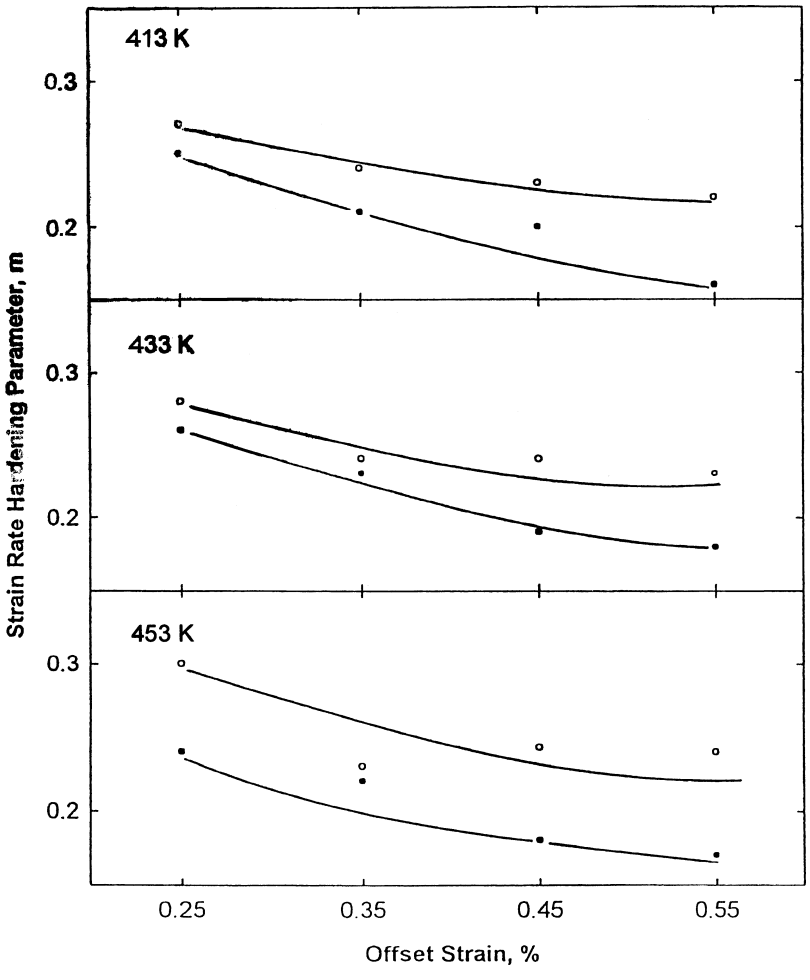

Figure 15 Effect of plastic offset strain on strain rate hardening parameter for the high and low flow stress 35 μm copper foils tested at (a) 413 K, (b) 433 K and (c) 453 K.

m foil. There is thus a strain/temperature window in which the foil types with high/low n and m values can be sorted.

4.6. m in elastoplastic regime

The strain rate change method for the characterization of m does not yield consistent results in the elastoplastic regime. Alternately, the constant strain rate elastoplastic σ-ε plots generated at different strain rates provide flow stress (σ) versus strain rate ($\dot{\varepsilon}$) data for a given strain level; the log σ versus log $\dot{\varepsilon}$ regression analysis yields an approximate measure of m. Here a clear trend for the variation of m with offset strain does not materialize; furthermore, the m characterized by this procedure is lower than that determined by the strain rate change method (in the post-yield regime). Table III shows the effect of grain size and test temperature on m averaged within the 0.05–0.25% offset strain range. The average m is larger for the finer grain structure and for the higher test temperature.

TABLE III Strain rate hardening parameter (m) for ED foils for strain $\varepsilon = 0.1$–0.3%

Foil Av. grain size (μm)	AM 0.3	Lo profile GR3 0.5	Hi profile GR3 2.0
296 K	0.075	0.041	0.028
373	0.099	0.065	0.043
453	0.136	0.096	0.063
473	0.144	0.104	0.080

5. Discussion

5.1. Elastic and elastoplastic parameters

Possible influences on the modulus behavior are on the one hand (a) strong effects of changes in crystallographic texture and (b) modifications of the interatomic bond strength related to thermal effect and structural defects (point defects and grain boundaries). On the other hand, important influences which occur only in the ED foil are porosity, three-dimensional vacancy agglomerates and possibly microcracks [40]. Whereas in the R foils the deformation induced vacancy type defects may anneal out or agglomerate to planar loops, in the ED foils an inherent high concentration of vacancies and voids [40] can be stabilized by hydrogen and swept up by grain boundaries during annealing [33, 34]. Another important difference between the two foil types is the stability of the crystallographic texture during annealing to 1173 K [35].

Several key findings concerning the elastic modulus of thin copper foil emerge in this study:

(i) Modulus for the *R* (TPC) foil is somewhat below that for the bulk polycrystalline copper [26] but it is significantly greater than that for the ED foils (Fig. 5).

(ii) The modest test temperature effect on modulus for the *R* (TPC) foil up to 573 K (Fig. 5) is similar to that for the bulk copper [26] but the effect is much smaller than that for the ED foils.

(iii) Annealing the *R* (TPC) foil to 873 K or the ED foils to 1173 K has little effect on modulus (Fig. 6) since neither foil type undergoes a texture transformation during thermal softening (modification of grain structure, reduction in dislocation density) or during subsequent grain growth.

(iv) The constancy of modulus with anneal temperature up to 873 K for the *R* (TPC), tough pitch copper, foil is apparently related to the 300–400 ppm oxygen present in the form of oxide particulates [35]. If the oxygen is reduced to less than 25 ppm, as for the (*R*) OFC foil, or if a few hundred ppm Ag is added to the *R* (TPC), as for the (*R*) Ag-TPC foil, the annealing has a considerable modulus lowering effect.

(v) A precipitous drop in modulus at temperatures above the anneal softening temperature for the *R* (OFC) and *R* (TPC) foils (Fig. 6), near 473 and 873 K respectively, is related to the crystallographic texture transformation to orientations near ⟨100⟩.

(vi) Since the anneal induced grain coarsening does not result in a significant modulus change (Fig. 6), the grain size effect on 23°C modulus and on temperature coefficient of modulus, as for the ED foils (Fig. 5), may be related to the deposition processing generated point defects "fingerprint" left in the foil [40], rather than to the grain size per se. However, the secondary effect of grain size on modulus is not discounted.

Indeed, the grain size affects the room temperature values of E (Fig. 5), σ_y and n (Fig. 7), E_t (Fig. 9) and m (Table III); the smaller grain size corresponds to the higher values for all parameters. Above 296 K, the thermal (test or anneal temperature) effects begin to dominate the grain size contribution. A large change in E, often over a relatively narrow range of temperatures, suggests a texture transformation (Fig. 6) whereas a large change in σ_y suggests a reduction in dislocation density (Fig. 12). The elastoplastic parameters n (Fig. 8) and E_t (Fig. 11) are influenced by a change in texture as well as in dislocation density, their relative contribution depending upon the strain level, and to a less extent by the modification of grain structure. For example, a large drop in E_t around 473 K for the OFC foil (Fig. 11) is apparently due to recrystallization as well as due to texture modification. An enhanced change of grain size for the ED samples with the smallest grain size (0.3 μm) is apparently responsible for the extraordinary drop in E_t with anneal temperature (Figs 9 and 10). The flow stress (Figs 13 and 14), m (Table III, Fig. 15) and n (Fig. 8) are postulated, as discussed in the following section, to relate to handling damage of the thin foil.

5.2. Relation to handling damage

The major use of thin copper foil is in the manufacture of printed circuit (wiring) board; the foil is laminated to the polymeric substrate (FR-4, polyimide) and is further processed (circuitization of conductor layer, lamination of cover layer, solder reflow), often at temperatures in excess of 413 K. The foil is prone to handling damage such as wrinkling, (impact) denting and micro-buckling at or above room temperature. The laminate, if improperly designed or processed, is prone to (particulate) denting and z-direction distortion such as warpage and curl during lamination (413–473 K) or during further processing (373–573 K).

Under the conditions of non-uniform loading, small scale wrinkles, buckles or dents initiate near the strain gradients at selected points on the foil [41]. At these points of instability, an elastic or elastoplastic collapse is brought on by the in-plane compressive stress [42]. The beneficial effects of σ_y (or flow stress), n and m in circumventing the localized small scale visible defects has been recognized [43, 44]. High σ_y or flow stress guarantees elastic recovery of defects or reduces the plastic strain; high E and E_t enhance the wrinkle modulus and hence the critical stress for initiating the microdefects [45]; high n results in a broader, more uniform distribution of strain in the presence of a stress gradient [46]; high m aids in resisting strain localiation during the development of instability [46]. An increase in n decreases the pre-instability (elastoplastic) strain gradients whereas an enhanced m decreases the post-instability (low strain plastic) strain gradients [47]. In particular, the role of m in retarding the growth of instability becomes greater as the foil thickness decreases [48, 49].

The thermal expansion differential between copper and substrate is the driver for distortion defects in the laminates and the multi-layer stacks. Given this differential, the extent of warp or curl depends upon thermal loading (temperature cycle, thermal stress), stack geometry, process controls and E, E_t for copper and substrate [32]. The warpage may occur during (i) lamination, (ii) circuitization of the copper layer by etching, (iii) reflow or infrared soldering and (iv) solder masking process. The three-dimensional thermoelastic or thermoviscoelastic models have been formulated [50] for a measure of warp and as an aid to laminate design. In the event of high thermal loading, E_t may be substituted for E but the viscoelastic or plastic relaxation (the reduction of thermal stresses) may occur at the peak lamination or soldering temperature, considerably complicating the analysis. The finite element analysis (FEA) models [51–53] effectively handle the complex design and processing details, and provide a more reliable quantitative measure of distortion and the cause/effect understanding of the underlying factors. Both the analytical and FEA modeling require "good" mechanical and thermal parameters and their temperature dependency, which we have shown in this study to be unique to each foil type.

This study is the pioneering effort in characterizing the mechanical parameters for the thin *R* and ED copper

foils over a range of temperatures of interest. Also underway is the measurement of thermal expansion behavior of the *R* and ED copper foils over a range of temperatures. These results will be reported in the near future.

6. Conclusions

(i) Elastic Regime: At 296 K, the E is inversely proportional to the grain size. For the *R* foil, the temperature dependency of E is similar to that for the bulk copper. For the ED foil, the temperature dependency is greater (than for the *R* foil) and it increases with the decreasing initial grain size; this grain size effect is assumed to be due to the point defects fingerprint unique to each ED foil. The post-anneal grain size has a relatively small effect on E except for the *R* foils where the anneal induced emergence of crystallographic textures near the ⟨100⟩ orientation results in a sharp drop in E; for the TPC foil the drop is near 873 K and for the OFC foil it is near 473 K. The foil thickness has a small effect on E.

(ii) Elastoplastic Regime: At 296 K, the values of E_t, σ_y, n and m are inversely proportional to the grain size; at higher temperatures, this grain size effect is dominated by the thermal effects. At 573 K, the foils have close σ_y and n, irrespective of the grain size. Both σ_y and n decrease with temperature; the drop in σ_y, due to the diminution of dislocation activity, is abrupt for the *R* foil and gradual over a wide range of anneal temperatures for the DF foil. The E_t decreases with strain and with temperature; this temperature effect on E_t is much greater than that on E. For the OFC foil, a large drop in E_t around 473 K is apparently due to recrystallization as well as due to texture modification. The m increases mildly with the test temperature.

(iii) Low Strain Plastic Regime: The m values for thin ED foils are significantly higher than those reported for the sheet in the higher strain regime; m decreases with strain and increases mildly with the test temperature. The flow stress, m and n, are postulated to relate to the handling damage of the thin foil.

Acknowledgements

R. Wiechmann (Gould) engaged the authors in stimulating and helpful discussions during various stages of this investigation. *E.* El-Magd performed the mechanical testing with the micro-tensile tester. M. Minor (Gould) performed the crosshead monitor tests in the low strain plastic regime and conducted the careful data analysis of all results. For partial financial assistance for one author (G. Khatibi), we like to thank the Austrian National Science Foundation, Project No. 14732 TEC.

References

1. M. Y. FUKS, L. S. PALATNIK, A. I. ILINSKII and V. V. BELOZEROV, *Sov. Phys.—Solid State* **9**(3) (1967) 588.
2. H. ASADA, Y. KISHI and Y. HIROSE, *Thin Solid Films* **236** (1993) 247.
3. M. ELENA *et al.*, *ibid.* **236** (1993) 209.
4. J. A. SCHWEITZ, *MRS Bulletin* **7** (1992) 34.
5. G. C. BROWN and R. J. PRYPUTNIEWICZ, *Proc. SPIE* **2004** (1993) 304.
6. J. MENCIK, E. QUANDT and D. MUNZ, *Thin Solid Films* **287** (1996) 208.
7. A. K. JAMTING, J. M. BELL, M. V. SWAIN and N. SCHWARZER, *ibid.* **308/309** (1997) 304.
8. A. ROUZAUD, E. BARBIER, J. EMOULT and E. QUESNEL, *ibid.* **270** (1995) 270.
9. M. F. DOERNER and W. D. NIX, *J. Mater. Res.* **1** (1986) 601.
10. D. SON, Y. H. LEE, J. H. AHN and D. KWON, in MRS Symp. Poc., Polycrystalline Metals and Magnetic Thin Films (1999) Vol. 562, p. 201.
11. M. V. SWAIN and J. MENCIK, *Thin Solid Films* **253** (1994) 204.
12. S. JAYARAMAN, R. L. EDWARDS and K. J. HEMKER, in MRS Symp. Proc., Thin Films—Stresses and Mechanical Properties (1998) Vol. 505, p. 623.
13. A. J. KALKMAN, A. H. VERGRUGGEN, G. C. A. M. JANSSEN and F.H. GROEN, *Rev. Sci. Instr.* **70** (1999) 4026.
14. H. J. READ and A. H. GRAHAM, *J. Electrochem. Soc.* **108** (1961) 73.
15. V. V. POLYAKOV and A. V. GOLOVIN, *Russian Met.* (4) (1995) 81.
16. A. NEUBRAND and P. HESS, *J. Appl. Phys.* **71** (1992) 227.
17. B. SCHULTRICH *et al.*, *Thin Solid Films* **253** (1994) 125.
18. H. COUFAL *et al.*, *J. Phys. III* (*Paris*) *Colloq.* C **74** (1994) 717.
19. H. MIZUBAYASHI, Y. YOSHIHARA and S. OKUDA, *Phys. Stat. Sol.* (a) **129** (1992) 475.
20. H. MIZUBAYASHI, T. YAMAGUCHI and Y. YOSHIHARA, *J. Alloys Compounds* **211/212** (1994) 446.
21. J. O. SKI, K. H. WU and G. LARKINS, *Mater. Charac.* **38** (1997) 301.
22. V. A. LAMB, C. E. JOHNSON and D. R. VALENTINE, *J. Electrochem. Soc.* **117** (1970) 291C; 341C; 381C.
23. A. FOX, *J. Testing Evaluation* **4** (1976) 74.
24. G. T. MEARINI and R. W. HOFFMAN, *J. Electronic Mats.* **22** (1993) 623.
25. C. Y. FU and C. UME, *JOM* **47**(6) (1995) 31.
26. W. H. MUNSE and N. A. WEIL, *ASTM Proc.* **51** (1951) 996.
27. V. KRSTIC, U. ERB and G. PALUMBO, *Scr. Metall. Mater.* **29** (1993) 1501.
28. W. C. OVERTON, JR. and J. GAFFNEY, *Phys. Rev.* **98** (1997) 969.
29. J. H. CHOI, S. Y. KANG and D. Y. LEE, *J. Mater. Sci.* **35** (2000) 4055.
30. B. C. HENDRIX, L. G. YU, K. W. XU and J. W. HE, MRS Symp. Proc., Polycrystalline Thin Films: Structure, Texture, Properties and Applications II (1996) Vol. 403, p. 171.
31. C. A. O. HENNING, F. W. BOSWELL and J. M. CORBETT, *Acta Met.* **23** (1975) 177.
32. G. KHATIBI *et al.*, Proc. Tech. Papers, IPC EXPO 2001, Anaheim, CA (2001).
33. H. D. MERCHANT, *J. Electronic Mats.* **22** (1993) 631.
34. *Idem.*, *ibid.* **24** (1995) 919.
35. H. D. MERCHANT, W. C. LIU, L. A. GIANNUZZI and J. G. MORRIS, to be published.
36. R. J. DEANGELIS, D. B. KNORR and H. D. MERCHANT, *J. Electronic Mats.* **24** (1995) 927.
37. M. ANWANDER, B. WEISS, B. ZAGAR and H. WEISS, in "Experimental Mechanics", edited by I.M. Allison (Balkema, Rotterdam, 1998) p. 692.
38. H. D. MERCHANT, *J. Electronic Mats.* **26** (1997) 833.
39. J. HEDWORTH and M. J. STOWELL, *J. Mats. Sci.* **6** (1971) 1061.
40. H. D. MERCHANT, "Defect Structure, Morphology and Properties of Deposits," edited by H.D. Merchant, *The Minerals, Metals and Materials Society Scientific Papers* (Warrendale, PA, 1995) p. 1.
41. K. YOSHIDA *et al.*, *Inst. Phys. Chem. Res.* **68**(3) (1974) 85.
42. H. HAYASHI *et al.*, *ibid.* **70**(3) (1976) 52.
43. A. M. SZACINSKI and P. F. THOMSON, *J. Mech. Working Tech.* **10** (1984) 87.
44. A. M. SZACINSKI and P. F. THOMSON, *Mats. Sci. Tech.* **7** (1991) 37; 224.

45. I. AOKI, T. MATOBA and M. ATAKA, in Proc. 12th Biennial Congress, Inter. Deep Drawing Research Group (Santa Margherta Lijure, Italy, 1982) p. 221.
46. A. K. GHOSH, Trans. ASME, *J. Eng. Mats. Tech.* **99** (1977) 264.
47. *Idem.*, *Met. Trans.* **5** (1974) 1607; **8A** (1977) 1221.
48. A. M. SZACINSKI and P. F. THOMSON, *Adv. Tech. Plasticity* **11** (1987) 1171.
49. R. MAHMUDI, *J. Mats. Processing Tech.* **37** (1993) 203.
50. J. H. LAU, "Thermal Stress and Strain in Micorelectronics Packaging" (Van Nostrand Reinhold, 1993) p. 883.
51. I. C. UME, T. MARTIN and J. T. GATRO, *IEEE Trans., CHMT*, Part A **20** (1997) 295.
52. G. J. PETRICCIONE and I. C. UME, *Advanced Packaging* **22** (1999) 125.
53. Y. POLSKY and I. C. UME, *J. Electron. Packaging* **121** (1999) 263.

Received 11 August
and accepted 12 March 2003